MONITORING GRASSLANDS USING CONVEX GEOMETRY AND PARTIAL UNMIXING – A CASE STUDY

Anne Jacobsen[1,2,3], Kathleen B. Heidebrecht[1] , Allan A. Nielsen[4]

[1]Center for the Study of Earth from Space/CIRES, Campus Box 216, University of Colorado, Boulder, CO 80309-0449 USA

[2]Institute of Geography, University of Copenhagen, Øster Voldgade 10, DK-1350 Copenhagen K, Denmark

[3]National Environmental Research Institute, Department of Landscape Ecology, Grenåvej 12, DK-8410 Rønde, Denmark

[4]Department of Mathematical Modeling, Technical University of Denmark, Building 321, DK-2800 Lyngby, Denmark

ABSTRACT

The main purpose of the study was to investigate if convex geometry and partial unmixing could be used to map succession stages on grasslands with respect to encroachment. The study was performed on a Compact Airborne Spectrographic Imager (*casi*) image acquired in 2 m resolution spatial mode with 11 bands in the spectral range from 396.2-902.6 nm. Spectral mode image data was used to assess the radiometric and spectral calibration and consequently the spatial data was spatially and spectrally subset to include 9 bands. The data were calibrated to surface reflectance and transformed to minimum noise fraction (MNF) feature space and the spectral dimensionality of the data was evaluated. Pixel purity indexing (PPI) technique was used to extract the purest pixels in the image from convex geometry concepts and rotating three-dimensional scatterplots were used to find endmember related to woody species. Two endmembers were identified: deciduous trees and conifers. Conifers were highly correlated with shade. Matched filtering or Constrained Energy Minimization (CEM) was used to map the selected endmembers. Forests with deciduous trees and conifers had high abundance. Groups of trees on derelict grassland areas where the density and age of trees were similar to the forests also had high abundance. Individual woody species out in the open grassland area had high abundance in a few places. Grassland areas with a spectral signature similar to conifers came out with low abundance and agricultural fields came out as false positives. It is generally concluded that the image gives the option of mapping succession at a late encroachment stage whereas individual scrubs at early encroachment stages tend to be overlooked.

KEY WORDS: Succession, encroachment stage, matched filtering, constrained energy minimization.

INTRODUCTION

Monitoring of grasslands is an important environmental and ecological issue in Denmark. Most of the countryside is or has been under plough for centuries and the Nature Protection Act places large emphasis on protecting the areas that are not cultivated.

One of the main issues to pursue in the monitoring of grasslands is the succession. One aspect of succession is the encroachment of shrubs and trees over time. If encroachment proceeds, the open grassland areas vanish and several protected plant species

In: *1st EARSel Workshop on Imaging Spectroscopy*, Remote Sensing Laboratories, University of Zürich, Switzerland, 6-8 October 1998, pp. 309-316. Eds. M. Shaepman, D. Schläpfer, and K. Itten.

will disappear. Accordingly, it is important to register the encroachment stage of grassland in order to use nature management to prevent the shrubs from taking over completely.

STUDY AREA AND IMAGE DATA

The study area Mols Bjerge is located in the eastern part of Jutland. The area has been protected by the Nature Conservation Act since 1976. It is a softly undulated moraine landscape with elevations from 50 to 130 m.a.s.l. Open grassland communities and coniferous and deciduous forest occupy the landscape. Encroachment occurs on the grasslands at different intensities and succession stages vary throughout the landscape. In summer 1997 several images were acquired over the area with the *casi* [7]. The image used in thestudy and the acquisition parameters is seen in figure 1.

Casi image acquired 10th June 1997, 11:47 local solar time
Location: Mols Bjerge, Denmark, 56 12 48 N, 10 31 58 E
Spatial resolution: 2 m, 512 pixels across track
Altitude: 1300 m
Flight direction: North 1° E

Spectral configuration:

Band	FWHM (nm)	Center wavelength (nm)
1	16.3	424.35
2	12.8	475.6
3	12.8	525.2
4	12.9	550.05
5	12.8	601.6
6	11.1	650.65
7	11.1	682.85
8	11.2	715.1
9	11.2	736.7
10	11.2	769.1
11	11.2	801.6

Figure 1: Study area, image acquisition parameters and spectral configuration.

METHODS

The method was based on the concepts of convex geometry and partial unmixing [2]. Apparent surface reflectance was retrieved and transformed into minimum noise fraction (MNF) feature space [5], [10] to assess the data dimensionality. Assuming that only linear mixing occurred, every pixel in the image was considered a mixture of the purest pixels and a pixel purity index (PPI) procedure was run on the data. Image endmembers related to woody species were selected from rotating three-dimensional scatterplots. Matched filtering was used to partially unmix the data. Calculations were performed by means of ENVI ver. 3.0 [1].

ASSESSING RADIOMETRIC AND SPECTRAL CALIBRATION

A *casi* image acquired on the same date but in spectral mode was used for evaluation of the spectral calibration [8]. The spectral mode was configured to 96 contiguous channels with a sampling interval of 5.4 nm and a FWHM of 5.8 nm in the spectral region from 394.3-904.3 nm. The spectral mode was recording every 9^{th} pixel across track as a raked image. Atmospheric modelling showed that the radiometric calibration was poor below 467 nm and at low signal levels [8]. This affected bands one and two in the spatial data and the two bands were excluded.

An oxygen-fitting algorithm [3], [4] identifying the band with the deepest absorption feature due to oxygen at 762 nm was applied on the spectral data [8]. The analysis showed that there was a problem with spectral calibration and alignment. Mean spectral calibration precision of 0.25 nm along track was exceeded in the most left 15 columns [8] and 135 pixels in the left part of the spatial image were excluded.

APPARENT SURFACE REFLECTANCE

Apparent surface reflectance was retrieved using a modified empirical line calibration [8]. The intercept in the calibration was obtained from a MODTRAN path radiance spectrum and the multiplication factors from image spectra and field spectra measured over a parking lot at the time of the flight.

MINIMUM NOISE FRACTION

MNF transformation whitens the noise and compresses the spectral information to fewer bands if the data are hyperspectral in nature – that is if the number of bands exceeds the number of spectral classes in the image. Noise statistics for MNF transformation were estimated from a subset of the image covering the whole swath and rather homogeneous grassland areas intersected by a few gravel roads. The noise statistics were calculated assuming that the spectral shift difference between one pixel and another pixel offset by one in the horizontal and the vertical direction was due to noise [1].

There was spectral information in every MNF band since spatial features were recognizable in every band. This may indicate that the image was spectrally underdetermined and that there may be more spectral variation in the image than the number of spectral bands can explain.

CONVEX GEOMETRY

The PPI was computed by repeatedly (in our case 20,000 iterations) projecting all observations in MNF space onto a random unit vector. A threshold of 2.5 digital numbers (1 digital number (DN) being equal to 1 standard devation from the pixel mean) selected the pixels on the ends of the projected vector. Pixels more extreme than 2.5 DN were considered to be noise pixels. The total number of times each pixel was marked extreme was calculated to construct the PPI image. Based on these extreme pixels rotating three-dimensional scatterplots were used to determine which extreme pixels belonged to which endmember. For each endmember the spectrum was calculated as the average of the extreme pixels belonging to that class.

The land cover types with the highest PPI scores were agricultural fields and forested areas with coniferous or deciduous trees. Pixels with the very highest scores were located in the surroundings of two farms and since the farms and the agricultural field were located in the top and the bottom of the image, the undesired extreme pixels were easily excluded from the PPI image

ENDMEMBER IDENTIFICATION

A scatterplot of the first three MNFs of the subset PPI image revealed that the shade was an overall dominating factor in the image. A shade endmember was selected from the scatterplot of the purest pixels. A match filtering (see below) result of abundance between 0.7 and 1 was masked from the original image and the PPI was run again. The final two endmembers were identified as deciduous forest (endmember 1) and coniferous forest (endmember 2) from a rotating three-dimensional scatterplot of the purest pixels of the second PPI result.

PARTIAL UNMIXING

The partial unmixing method applied is referred to as matched filtering or CEM [11], [13]. CEM builds on the usual linear mixture model

$$\mathbf{r}(x,y) = \mathbf{M}\,\boldsymbol{\alpha}\,(x,y) + \mathbf{n}(x,y)$$

where $\mathbf{r}(x,y)$ is an l by 1 vector of observations at location (x,y) (l is the number of spectral bands), $\mathbf{M}$ is an l by p matrix with columns containing the end-member spectra for the p end-members ($\mathbf{M}$ is constant for all (x,y)), $\boldsymbol{\alpha}(x,y)$ is a p by 1 vector of abundance for the end-members at location (x,y), and $\mathbf{n}(x,y)$ is an l by 1 vector of noise. In the model the noise is random with dispersion (or covariance) matrix $\sigma^2\,\mathbf{I}$ ($\mathbf{I}$ is the l by l unit matrix).

We split the $\mathbf{M}\,\boldsymbol{\alpha}$ term (we drop (x,y) from the notation) into two terms, one which is the desired end-member $\mathbf{d}$ with a corresponding abundance α_p (without loss of generality we place $\mathbf{d}$ in the last column of $\mathbf{M}$), and one which consists of the undesired end-members $\mathbf{U}$ with a corresponding (p–1) by 1 vector, $\boldsymbol{\gamma}$, of abundances. $\mathbf{U}$ contains the first (p–1) columns of $\mathbf{M}$ and $\boldsymbol{\gamma}$ contains the first (p–1) elements of $\boldsymbol{\alpha}$. Hence

$$\mathbf{r} = \mathbf{M}\,\boldsymbol{\alpha} + \mathbf{n} = \mathbf{d}\,\alpha_p + \mathbf{U}\,\boldsymbol{\gamma} + \mathbf{n}$$

We now project $\mathbf{r}$ onto $\mathbf{w}$ resulting in $\mathbf{w}^T\mathbf{r}$ with the intent to suppress the presence of the undesired end-members and to highlight presence of the desired end-member. We do this by minimizing the total output energy, E,

$$E = \Sigma\,(\mathbf{w}^T\mathbf{r})^2$$

where the sum over the squared projections is taken over all observations. At the same time we want the output to be one when the desired end-member is projected, $\mathbf{w}^T\mathbf{d} = 1$. To minimize E under the constraint $\mathbf{w}^T\mathbf{d} = 1$ we introduce a Lagrange multiplier 2λ and minimize

$$F = \Sigma\,(\mathbf{w}^T\mathbf{r})^2 - 2\lambda\,(\mathbf{w}^T\mathbf{d} - 1)$$

without constraints. This is done by setting the partial derivatives $\partial F/\partial \mathbf{w} = \mathbf{0}$ and $\partial F/\partial \lambda = 0$. This leads to

$$\mathbf{w} = \mathbf{R}^{-1}\,\mathbf{d} \,/\, \mathbf{d}^{T}\mathbf{R}^{-1}\,\mathbf{d}$$

(with $\lambda = 1 / \mathbf{d}^{T}\mathbf{R}^{-1}\,\mathbf{d}$) where $\mathbf{R} = \Sigma\, \mathbf{r}\, \mathbf{r}^{T}$ is the total sum of squares matrix.

Other techniques such as orthogonal subspace projection, OSP [9], [6], are also referred to as matched filtering. As opposed to CEM, OSP and full linear unmixing require knowledge of all end-member spectra. In [11] it is shown that full linear unmixing and OSP as described in [6] are identical (except that OSP is computationally slightly more expensive).

RESULTS AND DISCUSSION

Four subsets of the original image and abundance maps of endmembers 1 and 2 are seen in figure 2. The dark areas/pixels in the RGB images of all the subsets are coniferous forest/trees and the light red areas are deciduous forest/trees. The very red areas especially evident in subset 2 are deciduous scrubs.

Subset 1 illustrates that the two endmembers map the two types of forest well. Subset 2 shows that individual coniferous trees come out well at a late encroachment stage. Deciduous trees map too, but coherent deciduous scrubs are not mapped. Subset 3 shows again that trees at a late encroachment stage have high abundance but also that some areas that are shade come out as endmember 2. Subset 4 shows that only few individual bushes and trees out in the open grassland areas are mapped. Due to the spectral similarity between the dry, sparsely vegetated grassland and endmember 1, the endmember is mapped with relatively high abundance in subset 4.

CEM maps targets from their spectral characteristics without knowing the spectral characteristics of the background endmember. The match filtering minimizes the variance of the overall spectral response and gives unit scores only to perfect matches. The pixels that exist in sufficient quantity and with sufficient spectral contrast are the covariance drivers of the image statistics. Those spectra will be properly nulled and receive a near-zero filter response. Pixels that have a significant contrast but only exist in limited quantity will not be properly nulled and will be mapped as false positives. False positives occur in the agricultural fields, which get high abundance scores because we consider them as background (undesired endmembers) even though the fields spectrally speaking are endmembers.

CONCLUSION

Convex geometry concepts and matched filtering work well when the desired endmembers are the covariance drivers of the image statistics either because of their number or their spectral characteristics whereas rare objects must have a significant spectral signature to be identified. In a grassland environment where deciduous and coniferous forests occupy a large part of the landscape, scrub species and trees that exist only as individuals do not have a sufficient number or a significant spectral signature to be identified as endmembers. This influences grassland-monitoring results. Woody species encroaching from the forests map with high abundance on derelict old grasslands where the species are old (large) or make a coherent surface cover. Scrubs and trees that do not originate from the forests are not identified as endmembers and are only mapped if they have a spectral signature similar to the

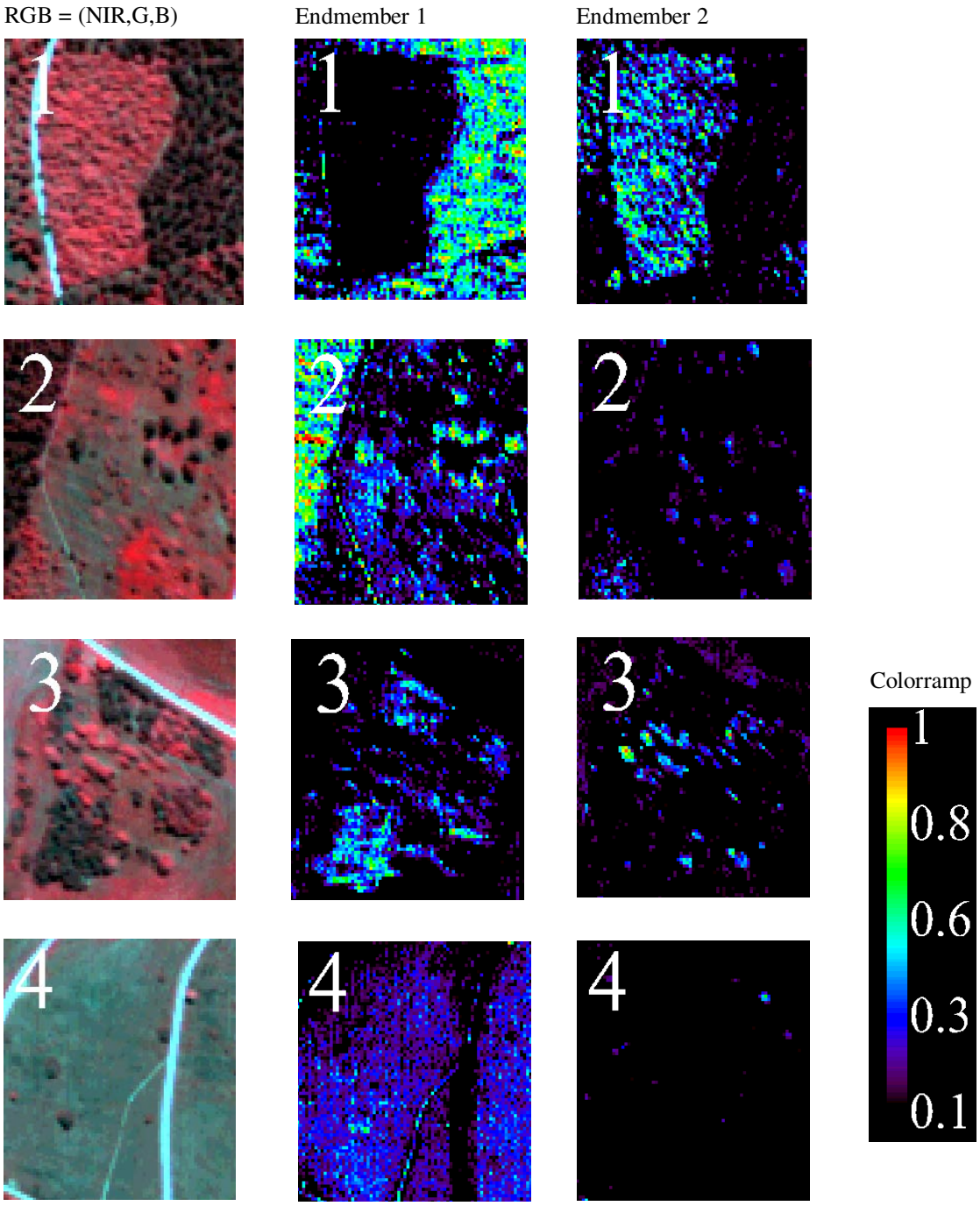

Figure 2: Four subsets showing the original image and match filtering results of endmember 1 (conifers) and endmember 2 (deciduous trees). See text for discussion.

forest species. This puts a limit to the monitoring of the general encroachment stage on grasslands but the abundance maps of the forest species become an important source for assessing the importance of biotope references to encroachment on derelict grasslands.

ACKNOWLEDGEMENTS

The study is part of the multidisciplinary research program DANMAC (DANish Multisensor Airborne Campaign) funded by the Danish Space Board.

The first author thanks the Director and scientists at Center for the Study of Earth from Space (CSES)/CIRES, University of Colorado at Boulder and their colleagues for scientific discussion, support and encouragement.

REFERENCES

[1] Better Solutions Consulting. ENVI User's Guide, the Environment for Visualizing Images, Version 3.0 Research Systems, Inc., and Better Solutions Consulting, 1997. Internet http://www.rsinc.com/.

[2] Boardman, Joseph W, Kruse, Fred A., Green, and Roberto O.. Mapping Target Signatures via Partial Unmixing of AVIRIS Data. Summaries of the Fifth Annual JPL Airborne Earth Science Workshop, January 23-26, 1995. Vol. 1. AVIRIS Workshop.

[3] Goetz, Alexander F.H., Heidebrecht, K.B. and Chrien, T.G.. High Accuracy in in-flight wavelength calibration of imaging spectrometry data, Proc. Fifth Annual JPL Airborne Geoscience Workshop, JPL Pub. 95-1:67-69, 1995.

[4] Goetz, Alexander F.H., Heidebrecht, Kathleen B.. Full-Scene, Subnanometer HYDICE Wavelenght Calibration, Proceedings SPIE, Vol. 2821, 1996.

[5] Green, Andrew A., Berman, Mark, Switzer, Paul and Craig, Maurice D.: A Transformation for Ordering Multispectral Data in Terms of Image Quality with Implications for Noise Removal. IEEE Transactions on Geoscience and Remote Sensing, Vol 26, No. 1, pp. 65-74, January 1988.

[6] Harsanyi, Joseph C. and Chang, Chein-I. Hyperspectral image classification and dimensionality reduction: An orthogonal subspace projection approach. IEEE Transactions on Geoscience and Remote Sensing, 32(4):779-785, 1994.

[7] ITRES Research Limited. Internet http://www.itres.com/.

[8] Jacobsen, A., Heidebrecht, K., Goetz, A.F. (subm.): Assessing the Radiometric and Spectral Calibration of CASI data and Retrieval of Surface Reflectance Factors. Photogrammetic Engineering and Remote Sensing.

[9] Miller, John W. V., Farison, James B. and Shin, Youngin. Spatially invariant image sequences. IEEE Transactions on Image Processing, 1(2):148-161, 1992.

[10] Nielsen, Allan Aasbjerg. Analysis of Regularly and Irregularly Sampled Spatial, Multivariate, and Multi-temporal Data. Ph.D. Thesis No. 6, Department of Mathematical Modelling, Technial University of Denmark.1994. Internet http://www.imm.dtu.dk/~aa/phd/.

[11] Resmini, R. G., Kappus, M. E., Aldrich, W. S., Harsanyi, J. C. and Anderson, M. Mineral mapping with HYperspectral Digital Imagery Collection Experiment (HYDICE) sensor data at Cuprite, Nevada, U.S.A. International Journal of Remote Sensing, 18(7):1553-1570, 1997.

[12] Settle, J. J.. On the relationship between spectral unmixing and subspace projection. IEEE Transactions on Geoscience and Remote Sensing, 34(4):1045-1046, 1996.

[13] Stan, Sorel S.. Mineral Identification and Mapping by Imaging Spectroscopy Data Analysis. PhD thesis, Computational and Applied Mathematics Department, University of the Witwatersrand, Johannesburg, South Africa, 1997.